ADVANCES IN ATMOSPHERIC SCIENCES, 2021

• **Letters & Notes** •

What Drives the Decadal Variability of Global Tropical Storm Days from 1965 to 2019?※

Yifei DAI[1,2], Bin WANG[*1,2,3], and Weiyi SUN[2,4]

[1]*Key Laboratory of Meteorological Disaster of Ministry of Education, and Earth System Modeling Center, Nanjing University of Information Science and Technology, Nanjing* 210044, *China*

[2]*International Pacific Research Center, University of Hawaii at Manoa, Honolulu, HI* 96822, *USA*

[3]*Department of Atmospheric Sciences, School of Ocean and Earth Science and Technology, University of Hawaii at Manoa, Honolulu, HI* 96822, *USA*

[4]*Key Laboratory for Virtual Geographic Environment. Ministry of Education; State Key Laboratory Cultivation Base of Geographical Environment Evolution of Jiangsu Province; Jiangsu Center for Collaborative Innovation in Geographical Information Resource Development and Application; School of Geography Science, Nanjing Normal University, Nanjing* 210023, *China*

(Received 20 October 2020; revised 30 December 2020; accepted 26 January 2021)

ABSTRACT

The tropical storm day (TSD) is a combined measure of genesis and lifespan. It reflects tropical cyclone (TC) overall activity, yet its variability has rarely been studied, especially globally. Here we show that the global total TSDs exhibit pronounced interannual (3–6 years) and decadal (10 years) variations over the past five-to-six decades without a significant trend. The leading modes of the interannual and decadal variability of global TSD feature similar patterns in the western Pacific and Atlantic, but different patterns in the Eastern Pacific and the Southern Indian Ocean. The interannual and decadal leading modes are primarily linked to El Niño-Southern Oscillation (ENSO) and Pacific Decadal Oscillation (PDO), respectively. The TSDs-ENSO relationship has been steady during the entire 55-year period, but the TSDs-PDO relationship has experienced a breakdown in the 1980s. We find that the decadal variation of TSD in the Pacific is associated with the PDO sea surface temperature (SST) anomalies in the tropical eastern Pacific (PDO-E), while that in the Atlantic and the Indian Ocean is associated with the PDO SST anomalies in the western Pacific (PDO-W). However, the PDO-E and PDO-W SST anomalies are poorly coupled in the 1980s, and this "destructive PDO" pattern results in a breakdown of the TSDs-PDO relationship. The results here have an important implication for seasonal to decadal predictions of global TSD.

Key words: tropical storm days (TSDs), interannual and decadal variations, El Niño–Southern Oscillation, Pacific Decadal Oscillation (PDO)

Citation: Dai, Y. F., B. Wang, and W. Y. Sun, 2021: What drives the decadal variability of global tropical storm days from 1965 to 2019? *Adv. Atmos. Sci.*, https://doi.org/10.1007/s00376-021-0354-1.

Article Highlights:

- The TSDs has a steady relationship with ENSO from 1965 to 2018, while the TSDs-PDO relationship shows a breakdown in the 1980s.
- TSD decadal variations in the Pacific and Atlantic-Indian Oceans are, respectively, associated with the PDO-E and PDO-W.
- The TSDs-PDO relationship breakdown in the 1980s is due to the decoupling of SST anomalies associated with the PDO-E and PDO-W.

1. Introduction

Tropical cyclones (TCs) threaten one-to-two billion people's daily lives worldwide each year and cause billions of dollars' economic loss (Webster et al., 2005; Peduzzi et al., 2012; Zhang et al., 2019). For example, Hurricane Katrina (2005) resulted in a death toll of 1833 and economic losses of more than $125 billion in the Gulf Coast region (Adeola and Picou, 2014). Even weaker storms like tropical depressions can cause human life losses in vulnerable societies (ECLAC, 2009). Improving TC prediction and mitigat-

※ This paper is a contribution to the special issue on the Climate Change and Variability of Tropical Cyclone Activity.

* Corresponding author: Bin WANG
Email: wangbin@hawaii.edu

ing TCs' societal and environmental impacts demands a better understanding of global TC variations in recent decades and their underlying causes.

Extensive research has been carried out to study the observed variations of TC activities on seasonal to multidecadal timescales (e.g., Wang and Chan, 2002; Wu et al., 2005; Chen et al., 2006; Frank and Young, 2007; Liu and Chan, 2008; Huang et al., 2011; Zhan et al., 2011; Vecchi et al., 2014; He et al., 2015). Numerous studies have pointed out that natural oscillations such as Indian Ocean dipole (IOD), Madden-Julian Oscillation (MJO), El Niño-Southern Oscillation (ENSO), Pacific Decadal Oscillation (PDO), and Atlantic Multidecadal Oscillation (AMO) have pronounced impacts on observed variations of TC activities (Singh, 2008; Klotzbach, 2014; Patricola et al., 2014; Caron et al., 2015; Girishkumar et al., 2015; Wang et al., 2019). Meanwhile, numerical models suggest that anthropogenic forcing exerts pronounced impacts on TC genesis worldwide but with large uncertainty among various models (Yu et al., 2010; Sugi et al., 2012; Balaguru et al., 2016; Murakami et al., 2020). A global study of observed TC activity is necessary to further understand the TC climate variability.

Tropical storm days (TSD) is a combined measure of genesis and lifespan, reflecting the TC population during the entire life cycle. Wang et al. (2010) analyzed the relationship between global TSD and sea surface temperature (SST) based on singular value decomposition (SVD) analysis. The first SVD mode revealed a connection between TSD and natural oscillations (PDO and ENSO), while the second SVD mode exhibited a connection between TSD and global warming. Murakami et al. (2020) further analyzed the impact of global warming on the global TSD based on the SVD method. PDO, ENSO, and global warming operate at different timescales; however, Wang et al. (2010) had not further discussed how these factors affect the global TC system by separating different timescales. Also, previous studies suggested that the impacts of large-scale natural oscillations on regional TC activities are interactive. For example, the ENSO's effect on TC genesis in the western North Pacific (WNP) and the North Indian Ocean (NI) changes with different PDO phases (Girishkumar et al., 2015; Zhao and Wang, 2016, 2019), and the ENSO events can regulate the relationship between MJO and TC activity in the south Pacific (SP) and the North Atlantic (NA) (Chand and Walsh, 2010; Klotzbach and Oliver, 2015). However, we know little about whether there is any such interaction among the global TC activity's fundamental drivers.

The present work aims to address what drives the global TSD changes during the recent half-century and how these fundamental drivers affect global TSD on different timescales. Section 2 describes the data and methodology used in this study. Section 3 documents variations of global TSD in interannual and decadal time scales and explores the plausible large-scale environmental control of the worldwide TSD variability. In section 3, we are trying to address two specific questions: 1) How does global TSD change on different timescales? 2) What controls the variations of global TSD on different timescales? Summary and discussions are presented in section 4.

2. Data and Method

2.1. *Data*

The observational TC record used in this study is derived from the International Best Track Archive for Climate Stewardship, version 4 (IBTrACS v4; Knapp et al., 2010, 2018), for the period May 1965 to April 2019. The combined observational TC data is flagged as "USA agencies" in the IBTrACS v4, which includes the Joint Typhoon Warning Center (JTWC), Central Pacific Hurricane Center (CPHC), National Hurricane Center (NHC), and two World Meteorological Organization (WMO) Regional Specialized Meteorological Centers at Miami and Honolulu. The IBTrACS v4 dataset and its detailed information are available on the website: https://www.ncdc.noaa.gov/ibtracs/index.php?name=ib-v4-access; last access: 23 September 2020. Following Wang et al. (2010), we chose the data starting from 1965 when satellite monitoring of TC events became available to diminish the undesirable effect of missing cyclones.

Monthly mean sea surface temperature (SST) is derived from the National Oceanic and Atmospheric Administration (NOAA) Extended Reconstructed SST version 5 (ERSST v5, Huang et al., 2017). Pacific Decadal Oscillation (PDO) index (Mantua et al., 1997; Newman et al., 2016) and Niño-3.4 index used in this study are obtained from the NOAA Earth System Research Laboratory website: https://psl.noaa.gov/data/climateindices/list/; last access: 23 September 2020. Both PDO and Niño-3.4 indexes are diagnosed from ERSST v5 SST.

2.2. *Methodology*

The TSD defines the frequency of occurrence (days) of all tropical cyclones reaching and exceeding the tropical storm (TS) intensity, i.e. the one-minute sustained surface wind reaches 34 knots or greater. Compared with the criteria of surface wind speed (≥ 20 knots) used in Wang et al. (2010), the observation record for TS (≥ 34 knots) is more reliable. Because we only use TC positions reported every 6 hours (4 times a day), each record represents 0.25 days. To analyze the spatial-temporal variation of TSD, we transformed the raw data into a 2.5° × 2.5° grid by counting TSD at each grid. A 9-point weighted smoother is then applied to improve spatial continuity, while the weights are calculated based on the inverse distance interpolation algorithm of Lu and Wong (2008).

The 4-year running mean is used in this study to separate the interannual and decadal component of the global TSD. The 4-year running mean is a widely used convention to identify decadal variability in previous studies (e.g., Van Oldenborgh et al., 2012; Wang et al., 2018). The 4-year running mean time series represent the decadal variation compon-

ent, and the interannual variation component is obtained by subtracting the 4-year running mean time series from the original time series. The half-point of the response function for the 4-year running mean filter is around eight years; therefore, the interannual signal is largely removed (Wang et al., 2013). For the 4-year running mean time series, the yearly mark represents the second year of the 4-year mean period.

Empirical orthogonal function (EOF) analysis decomposes the temporal-spatial variation into a series of temporal-spatial orthogonal modes according to the eigenvalues and eigenvectors of the covariance matrix computed from the original dataset (Lorenz, 1956). Each leading EOF mode is described by a spatial pattern and a time-varying sequence (also known as the principal component, PC). The eigenvectors rank the EOF modes and the first leading EOF mode accounts for the largest covariance of the original dataset. This study applies the EOF method to normalized 3-dimensional fields of the global TSD and its decadal and interannual variation components. The North's test is used to examine the separability of each leading EOF mode (North et al., 1982). The statistical significance of linear correlation coefficients is determined by the effective degrees of freedom, which consider autocorrelation sequences with a lagged window (Bretherton et al., 1999; Xiao and Li, 2007).

3. Results

3.1. *Climatology and variability of the global TSD*

TSD is a useful metric to represent the overall TS activities. We computed the correlation coefficients among different TC indices [Table S1 in the electronic supplementary material (ESM)], including TSD, TS genesis number (TSG), power dissipation index (PDI; Emanuel, 2005), accumulated cyclone energy (ACE; Bell et al., 2000), and the average TS lifespan (LS). The TSD is highly or well correlated with other indices ($r > 0.69$), which is the best measure of TC activities among all the listed indices.

On average, a total of 408 TSDs is observed each year globally, which means that, on average, TS are seen every day over the global oceans. Seasonally, the total global number of TSD shows a maximum in September (78) and a minimum in May (18) (Fig. 1a), which results from an alternate occurrence of the TC seasons in the Northern Hemisphere (NH) and Southern Hemisphere (SH). To facilitate the study of the year-to-year variability of global TSD, Wang et al. (2010) define a "tropical storm year" as the yearlong period starting from 1 May to the following 30 April, which includes the NH TS season from 1 May to 31 November followed by the SH TS season from 1 December to the next 30 April. Hereafter, the year mentioned in this work is the TS year, not the calendar year.

Climatological mean distribution of TSD is primarily confined to the zonal belts of 10°–30°N and 10°–30°S except in the WNP and the NA regions where TSD occurrence extends north of 45°N (Fig. 1b). The highest frequency of TS exceeding one day per year is seen off the west coast of Mexico near (15°N, 110°W). A second center with TSD > 0.8 days per year is found over the Philippine Sea centered at (15°N, 130°E). The Pacific Ocean hosts 62% of the total global TSDs, including 34.2% in the WNP, 17.8% in the eastern north Pacific (ENP), and 10.0% in the SP. About 15.7% and 18.6% of the total global TSDs occur in the NA and the SI regions, respectively, and only 3.7% occurs in the NI.

The global total of TSD shows large amplitude year-to-year variations (Fig. 2a) with the maximum of 603 TSDs observed in the TS year of 1996 and the minimum of 287 TSDs in the TS year of 1977. However, no significant long-term trend is detected in the year-to-year variation of global TSD during the entire 54-year period (1965–2018), although the global mean surface air temperature has risen by about 0.96 degrees (Fig. 2a1). Further examination of the long-term trend of total TSDs in each ocean basin indicates that only the TSD in the NA region has a significantly increasing trend, which is 9.7 days (or 15%) per decade. The results here corroborate that of Murakami et al. (2020), in which the increasing trend is attributed to global warming. However, previous studies also pointed out that TC activity in the NA region is associated with the Atlantic multidecadal variability (AMV) (Delworth and Mann, 2000; Klotzbach and Gray, 2008). In this study, the number of NA TSD is also highly correlated with the AMV ($r = 0.85$ on the decadal timescale). Therefore, whether the AMV or global warming causes the NA TSD change remains uncer-

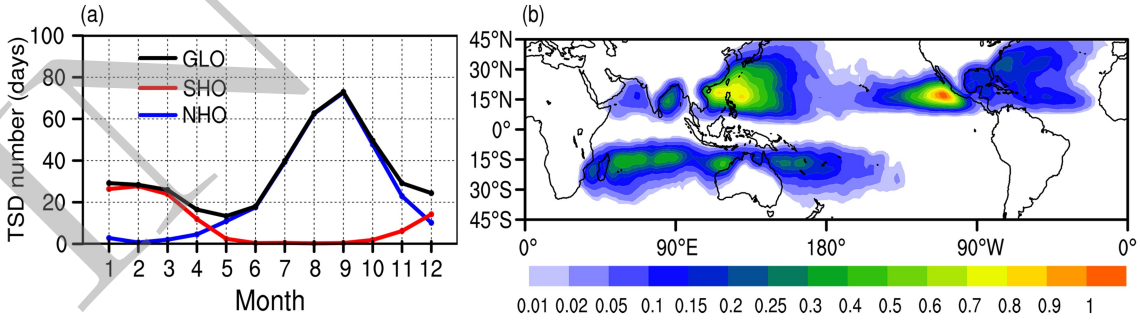

Fig. 1. TSD climatology. (a) Seasonal variation of TSD (days) averaged over the globe (black curve), Northern Hemisphere (NH, blue curve), and Southern Hemisphere (SH, red curve). (b) The spatial distribution of climatologically annual mean TSD (1965–2018).

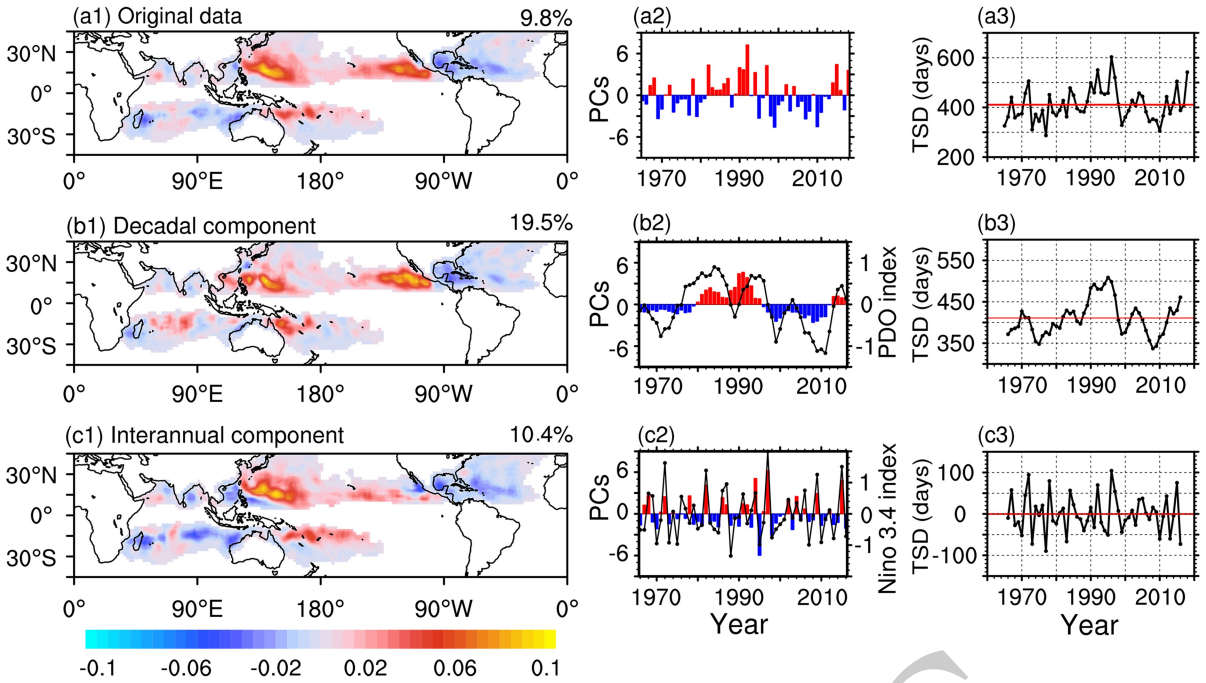

Fig. 2. Leading EOF modes of annual TSD variation. Left panels are the spatial distributions of the first EOF mode of TSD variation: (a1) Annual total TSD, (b1) decadal component (4-year running mean), and (c1) interannual component (total minus 4-year running mean) of the annual TSD. These modes are significantly separated from the rest of the EOFs. The corresponding percentage variance is shown on the top-right of each panel (a1, b1, and c1). The bar charts in the middle panels (a2, b2, and c2) represent the corresponding PCs of the EOF modes. The black curves in panel b2 and c2 represent the decadal component of the PDO index and the interannual component of the Niño-3.4 index, respectively. The Right panels show the time series of global TSD from the TS year of 1965 to 2018. (a3) Original TSD, (b3) Decadal component, and (c3) Interannual component. The red lines in a3, b3, and c3 represent corresponding mean values.

tain due to the limited length of available TC data.

The time series of the total global TSD is comprised of both interannual and decadal signals. To better understand what drives the TSD variations on the interannual and decadal timescales, separately, we followed the conventional method applying a 4-year running mean to get the decadal variability (DV) component and the interannual variability (IAV) components (the original TSD subtracted from the 4-year running mean). The IAV and DV components of global TSD are shown in Fig. 2. The IAV has significant 3-year and 6-year peaks, while the DV shows a significant 10-year peak with an insignificant 25-year signal [Fig. S1 in the electronic supplementary material (ESM)]. The ranges (maximum minus minimum) of the DV and IAV components are comparable, which are 171 and 194 days, respectively. Obviously, the highest TSD year (1996) and the lowest TSD year (1977) appear to be closely related to the maximum and minimum DV of the TSD.

The first leading modes of the IAV and DV components of the global TSD, denoted by IAV1 and DV1, both feature a large-scale contrast between the Pacific and the NA regions, i.e., positive TSD change in the Pacific and negative TSD change in the Atlantic (Fig. 2). Note, however, that the positive TSD anomalies in the eastern Pacific in DV1 are stronger and closer to the Mexican coast, while that in IAV1 is significantly weaker and more toward the central Pacific. In the Indian Ocean, the DV1 is dominated by positive TSD anomalies, while IAV1 is dominated by negative TSD anomalies, although the patterns in the Indian Ocean are not uniform. The first leading EOF mode of the total TSD (Fig. 2a1) shows a combined structure of DV and IAV that is similar to Wang et al. (2010). The PC is significantly correlated with the total global TSDs ($P < 0.01$) at multiple timescales ($r = 0.64$ for original data, $r = 0.69$ for DV1, and $r = 0.48$ for IAV1). Although the spatial pattern of the first leading EOF mode is not uniform, the PC1, to some extent, can represent the global TSD change, especially on the decadal timescale. The second leading EOF mode of the IAV component of global TSDs does not pass North's test (North et al., 1982). Therefore, the EOF modes following the leading EOF modes are not further discussed in this study.

3.2. *What drives the variations of the global TSD over the past 55 years?*

We noticed that the decadal PC1 is significantly related to the PDO index with a correlation coefficient of 0.64 ($P < 0.01$; the effective degrees of freedom is 19; Bretherton et al. 1999), while the interannual PC1 is more significantly correlated with the Niño-3.4 index with a correlation coefficient of 0.78 ($P < 0.01$). The Niño-3.4 index has significant peaks every 3–5 years (Fig. S2a). The PDO index has a

decadal oscillation of about ten years (Fig. S2b in the ESM), which corresponds fairly well to that of global TSD (Fig. S1 in the ESM).

The IAV1-ENSO relationship and the DV1-PDO relationship can be confirmed by the sea surface temperature (SST) anomaly patterns associated with the two leading modes. The regressed SST with reference to the decadal PC1 (Fig. S3b in the ESM) corresponds fairly well to that from the PDO index (r = 0.93). On the interannual timescale, the regressed SST on the interannual PC1 (Fig. S3c) is in good agreement with that associated with the Niño-3.4 index (r = 0.97).

Previous studies pointed out that PDO warm phase and El Niño events can modulate the atmospheric circulations (e.g., vertical wind shear, relative vorticity, and vertical velocity), causing an increase of TS genesis in the central Pacific and a reduction of TS genesis in the NA (Chen et al., 1998; Wang and Chan, 2002; Li and Zhou, 2012). The increased TSs in the southeast WNP move northwestward and experience long recurving tracks and lifespans (Chan 1985; Wang and Chan, 2002, Camargo et al., 2007a, b). Therefore, over the western Pacific, the TSD shows significant correlations with PDO and ENSO despite that the total TS genesis number does not (Fig. S4 in the ESM).

Are the global TSDs-ENSO and TSDs-PDO relationships stable during the whole period from 1965 to 2018 TS year? On the interannual timescale, the leading mode is strongly related to the Niño-3.4 index with positive correlation coefficients significant at the 99% confidence level during the entire period (Fig. 3a). Interestingly, on the decadal timescale, the significant correlation between PDO and DV1 broke down during the 1980s (Fig. 3a).

3.3. *Why did the TSDs-PDO relationship break down in the 1980s?*

It is interesting to note that both the warm phases of ENSO and decadal PDO are correlated with positive SST anomalies over the Pacific cold tongue (CT) region (5°S–5°N, 90°W–180°). Hereafter we refer to this region as the cold tongue (CT) following Zhang et al. (1997). The CT SST is highly correlated with the Niño-3.4 index with a correlation coefficient of 0.98. Also, Zhang et al. (2018) pointed out that the tropical SST contributes to part of PDO variability. The decadal variation of the CT SST acts as a "bridge" to link the ENSO and PDO. The decadal variation of the CT SST has the same magnitude as the PDO, but only one-third of the magnitude of ENSO variation.

To explore how PDO influences the decadal variation of global TSD, we decomposed the PDO signal into two components. The first PDO component is measured by the 4-year running mean of CT SST anomalies, which primarily represents the PDO positive SST anomalies in the tropical eastern Pacific triangle region (Wang et al., 2013). For this reason, it is named PDO-E (Fig. 4a). The PDO-E reflects the part of PDO that is linked to ENSO. On the decadal timescale, the PDO-E accounts for 39% of the total variance of PDO. The second PDO component is defined by the remaining SST anomalies obtained after the SST anomalies associated with the PDO-E are removed by using the partial correlation method. The second PDO component primarily represents the negative SST anomalies in the western Pacific K-shape region (Wang et al., 2013); so, it is named PDO-W (Fig. 4b). To represent the PDO-W SST anomalies more straightforwardly, we defined a new PDO-W index by the negative SST anomalies averaged over the WNP (30°–40°N, 160°E–160°W). The correlation map between this PDO-W index and global SST is highly consistent with the partial correlation map shown in Fig. 4b, with the pattern correlation coefficients being 0.98.

To identify the roles that PDO-E and PDO-W might play in the TSDs-PDO relationship, we further analyzed the correlation maps of TSD with reference to the PDO-E and PDO-W on the decadal timescale, respectively (Fig. 4c, and d). The PDO-E explains reasonably well the DV1 mode's spatial distribution in the increased TSD in the west-central North Pacific. In general, the PDO-E explains more than

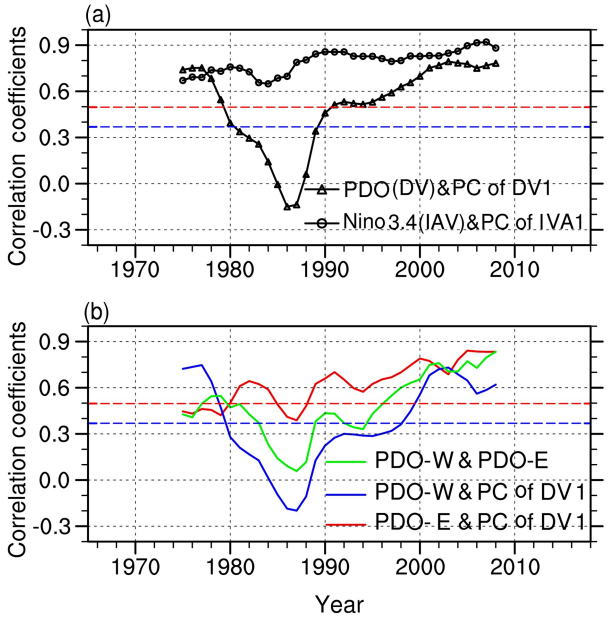

Fig. 3. Time series of 21-year sliding correlation coefficients among PDO, Niño-3.4, and TSD. (a) The black curve with triangles represents the correlation between the decadal variation of PDO and DV1 PC, whereas the black curve with circles represents the correlation between the interannual variation of Niño-3.4 index and IAV1 PC. (b) The blue curve represents the correlation between the decadal variation of PDO-W and DV1 PC; the red curve represents the correlation between the decadal variation of PDO-E and DV1 PC; the green curve represents the correlation between the decadal variation of PDO-W and PDO-E. The effective degrees of freedom is 19 on the interannual timescale, but is 10 on the decadal timescale according to Bretherton et al. (1999). The blue dashed line indicates that the correlation coefficients on the interannual timescale are statistically significant at the 90% confidence level, and the red dashed line indicates that the correlation coefficients on the decadal timescale are statistically significant at the 90% confidence level.

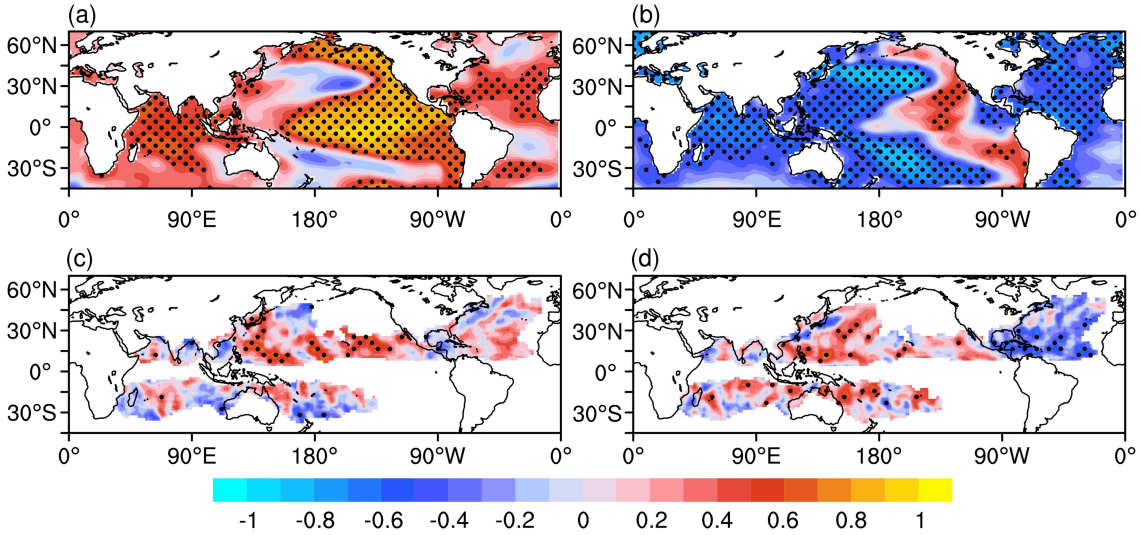

Fig. 4. SST anomaly patterns associated with the two components of the PDO. (a) the correlation map between the PDO-E index and SSTA on decadal timescale, and (b) same as in (a) but between PDO index and the SSTA with the influence of PDO-E removed on decadal timescale. The bottom two panels are the correlation map between (c) global TSD and PDO-E and (d) PDO-W, respectively. Dots indicate that the correlation coefficients are statistically significant at the 95% confidence level. The effective degree of freedom on the decadal timescale is 19 calculated based on the method in Bretherton et al. (1999).

two-thirds of the TSD change of the DV1 mode, and thus the temporal variation of PDO-E shows a good relationship with DV1 (Fig. 3b). On the other hand, the PDO-W primarily contributed to decreased TSD in NA and increased TSD in Southern Oceans, although it also contributes to increased TSD in the WNP.

Previous studies suggested that El Niño events and PDO warm phases can weaken and shift the Walker Circulation eastward, resulting in reduced TC activity in the NA and increased TC activity in the central Pacific (Chan, 1985; Klotzbach, 2011; Boudreault et al., 2017). The anomalous Walker Circulation regressed with reference to DV1 PC features ascending motion in the central Pacific and subsidence in the NA and the Maritime Continent regions (Fig. 5a1). This picture can be regarded as the circulation pattern associated with the DV1 mode, suggesting the same mechanism may operate as that discussed in previous studies. The PDO regressed fields (Figs. 5a2 and 5b2) correspond fairly well to the DV1 mode associated patterns. It explains how PDO affects the DV1 mode by modulating atmospheric circulation. Furthermore, the enhanced ascending motion in the central Pacific and subsidence near the Maritime Continent are related to the PDO-E but not the PDO-W. In contrast, the subsidence in the NA is related to the PDO-W but not the PDO-E (Figs. 5a3 and 5a4). The regressed vertical velocity shows the same features as the Walker Circulation (Figs. 5b2, 5b3, and 5b4). The circulation variabilities associated with the PDO-W and PDO-E suggest that the TSDs-PDO relationship results from the joint influence of PDO-E and PDO-W SST anomalies.

We now address why the TSDs-PDO relationship broke down in the 1980s in terms of PDO-E and PDO-W and their connection. Figure 3b shows that the PDO-E is well correlated with DV1 during the entire period (red curve), suggesting that the PDO-E SST anomalies always positively contributes to the TSDs-PDO relationship. On the other hand, the PDO-W and DV1 show a significant negative correlation during the 1980s (blue curve). The negative correlation period coincides with the period of TSDs-PDO relationship breakdown. The correlation between PDO-W and DV1 suggests that the PDO-W SST anomalies did not have a positive contribution during the 1980s, and that they may have played a destructive role in the TSDs-PDO relationship.

On the decadal timescale, the correlation between PDO-W and PDO is (0.87) higher than that between PDO-E and PDO (0.36), implying that the PDO-W primarily represents the PDO variation. Therefore, when the PDO-W has a poor relationship with PDO-E as it did during the 1980s (green curve in Fig. 3b), the PDO signal would primarily show the PDO-W features rather than PDO-E. A poor relationship between the two components of PDO is named the "destructive PDO pattern" shown in Fig. S5c. The "destructive PDO pattern" happened during the PDO warm phase. Figure 5 shows the differences of Walker Circulation and vertical velocity between the PDO warm phase (destructive PDO period removed) and PDO cold phase (Figs. 5a4 and 5b4) and between the "destructive period" and remained PDO warm phase (destructive period removed). The composite differences of the warm minus cold phase exhibit similar spatial patterns to the regressed fields by PDO and DV1 PC, while the differences of the destructive period minus warm phase exhibit the features of PDO-W that weaken the impact of PDO warm phase on the Pacific but strength the impact on the NA. Consequently, the "destructive PDO pattern" cannot fully explain the DV1 mode in the Pacific,

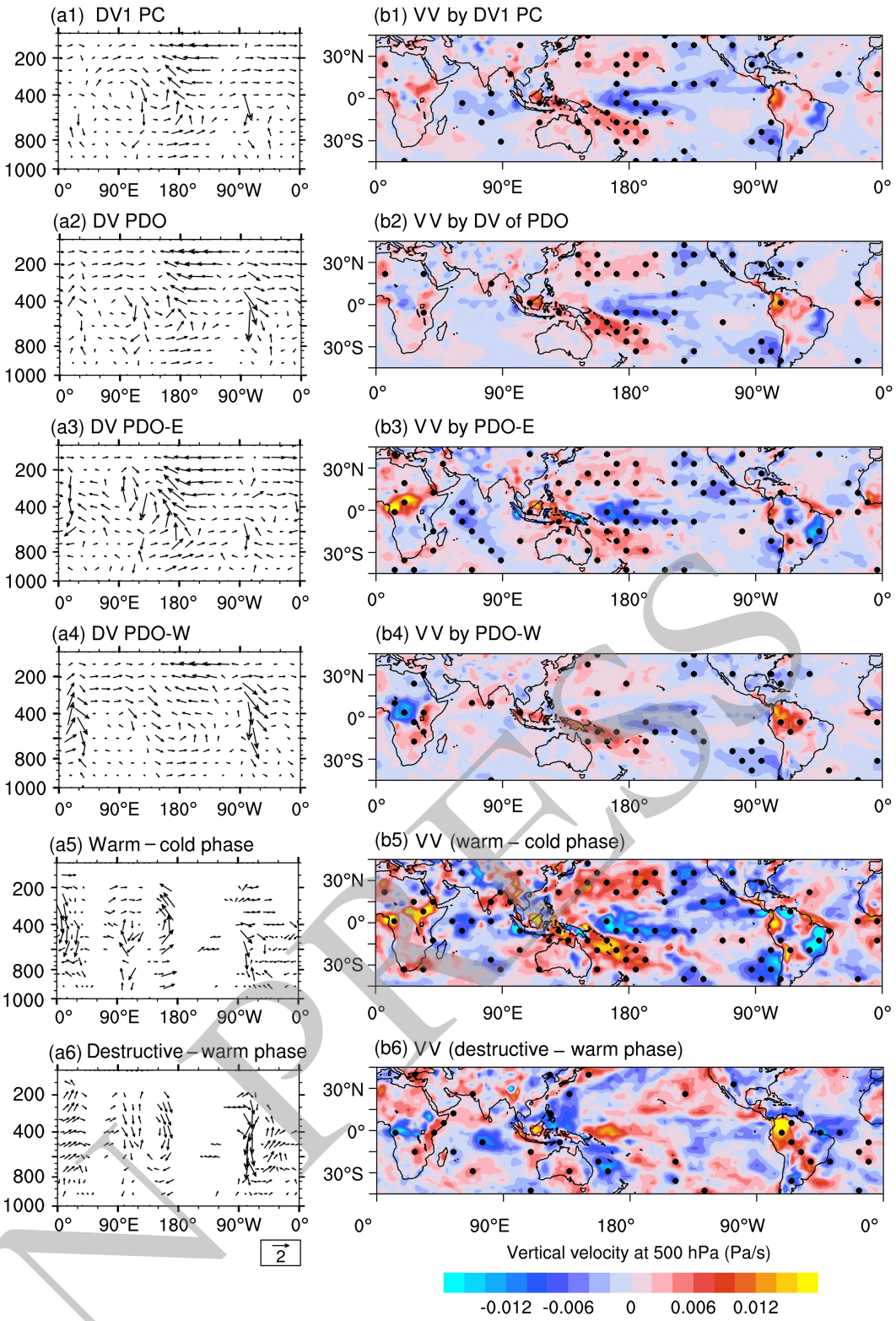

Fig. 5. The regressed Walker Circulation (a1–a4) and vertical velocity at 500 hPa (b1–b4, Pa s^{-1}) with DV1 (a1, b1), decadal variation of PDO (a2, b2), PDO-E (a3, b3), and PDO-W (a4, b4). The composite differences of Walker Circulation (a5, a6) and vertical velocity at 500 hPa (b5, b6) by the PDO warm phase (with the destructive period from 1983 to 1989 removed) minus PDO cold phase (a5, b5) and by destructive period minus PDO warm phase (with the destructive period removed) (a6, b6). The Walker circulation is composed of zonal wind (m s^{-1}) and vertical velocity (Pa s^{-1}), while the vertical velocity is multiplied by a scale factor that calculated as mean zonal wind speed divided by mean vertical velocity. Only significant circulation is shown in a1–a6.

where about two-thirds of the global TSD occurs, and thus results in a poor relationship between the PDO index and DV1 of TSD during the 1980s.

4. Summary and discussion

TSD is a combination of genesis and lifespan. Compared with the TS genesis, TSD contains more information about TS activity and shows better correlations with other TS indices (Table S1 in the ESM). However, most TC studies have focused on the genesis, intensity, and track changes. Only a few studies have dealt with tropical storm day variability.

On average, a total of 408 TSDs were observed each year, which primarily occurs in the zonal belts of 10°–30°N and 10°–30°S. While the total global TS genesis number fluctuated moderately from year to year, the global TSDs showed relatively larger-amplitude variations ranging from 287 to 603 TSDs, suggesting that the TC life span has more significant variability than does the TCG number. However, no significant long-term trend in the total global TSDs was found during 1965–2020. Instead, pronounced interannual (3–6 years) and decadal (10 years) variations were detected (Fig. S1 in the ESM). The interannual and decadal variabilities showed similar amplitudes; both are critical to account for the total TSD variation.

The first leading EOF modes of the interannual and decadal variability of global TSD featured similar patterns in the western Pacific and Atlantic, but different patterns in the Eastern Pacific and Southern Indian Ocean (Fig. 2). The leading interannual and decadal modes are primarily driven by ENSO and PDO, with significant correlations between the corresponding PCs and Niño-3.4 (r=0.78) and PDO indices (r=0.64) (Fig. 2). The significant relationship between the Niño-3.4 index and the TSD leading mode of interannual variation was robust during the entire period. In contrast, the TSDs-PDO relationship on the decadal timescale experienced a breakdown during the 1980s (Fig. 3a).

To understand how PDO affects global TSD change, we decomposed the overall PDO SST anomalies into two components, PDO-E and PDO-W. The PDO-E measured by the cold tongue (CT) SST anomalies reflects the part of PDO linked to ENSO. The PDO-W is the remaining PDO anomalies after the PDO-E is removed, reflecting the opposite-sign SST anomalies in the western Pacific (Figs 4a and 4b). The PDO-W can be measured by the negative value of SST anomalies over the WNP (30°–40°N, 160°–160°W). The PDO-W was primarily responsible for the decreasing TSD in the NA, while the PDO-E contributed most to the increasing TSD in the North Pacific (Figs. 4c and 4d). During the 1980s, a poor relationship between PDO-E and PDO-W, i.e., the "destructive PDO pattern", caused a breakdown of the TSDs-PDO relationship.

Previous studies found that ENSO and PDO can affect basin-scale TS activities by altering large-scale atmospheric conditions (Zhao et al., 2010; Zhan et al., 2011; Xiang and Wang, 2013). This study further identified the ENSO and PDO's fundamental roles in the global TSD change in multiple timescales. So far, it has been determined that the large-scale natural oscillations (ENSO and PDO), rather than global warming, primarily modulate the observed global TSD change. Also, the DV1 and IAV1 explained fractional variances are relatively low, indicating that TC activities contain considerable sub-basin-scale variabilities. Therefore, regional-scale studies are necessary for TSD change.

Previous studies pointed out that different PDO or AMO phases could affect the relationship between ENSO and TS activities in some regions via modulating climate regimes (Klotzbach, 2011; Girishkumar et al., 2015; Zhao and Wang, 2019). However, after distinguishing interannual and decadal signals, we found that different PDO phases have a negligible impact on the TSDs-ENSO relationship on the global scale. The findings here are helpful for understanding how TSD changed worldwide during the recent half-century, which has a significant implication for seasonal to decadal predictions of global TSD.

Acknowledgements. Bin WANG is supported by the National Science Foundation (Climate Dynamics Division) Award # NSF 2025057 and the National Natural Science Foundation of China (Grant No. 91437218). We acknowledge the High-Performance Computing Center of Nanjing University of Information Science & Technology for their support of this work. This paper is the IPRC publication #1503, SOEST publication #11239, and ESMC publication #344.

Electronic supplementary material: Supplementary material is available in the online version of this article at https://doi.org/10.1007/s00376-021-0354-1.

REFERENCES

Adeola, F. O., and J. S. Picou, 2014: Social capital and the mental health impacts of Hurricane Katrina: Assessing long-term patterns of psychosocial distress. *International Journal of Mass Emergencies and Disasters*, **32**(1), 121–156.

Balaguru, K., G. R. Foltz, L. R. Leung, and K. A. Emanuel, 2016: Global warming-induced upper-ocean freshening and the intensification of super typhoons. *Nature Communications*, **7**(1), 13670, https://doi.org/10.1038/ncomms13670.

Bell, G. D., and Coauthors, 2000: Climate assessment for 1999. *Bull. Amer. Meteor. Soc.*, **81**(6), S1–S50, https://doi.org/10.1175/1520-0477(2000)81[s1:CAF]2.0.CO;2.

Boudreault, M., L.-P. Caron, and S. J. Camargo, 2017: Reanalysis of climate influences on Atlantic tropical cyclone activity using cluster analysis. *J. Geophys. Res.*, **122**(8), 4258–4280, https://doi.org/10.1002/2016JD026103.

Bretherton, C. S., M. Widmann, V. P. Dymnikov, J. M. Wallace, and I. Bladé, 1999: The effective number of spatial degrees of freedom of a time-varying field. *J. Climate*, **12**(7), 1990–2009, https://doi.org/10.1175/1520-0442(1999)012<1990:TENOSD>2.0.CO;2.

Camargo, S. J., A. W. Robertson, S. J. Gaffney, P. Smyth, and M. Ghil, 2007a: Cluster analysis of typhoon tracks. Part I: Gen-

eral properties. *J. Climate*, **20**(14), 3635–3653, https://doi.org/10.1175/JCLI4188.1.

Camargo, S. J., A. W. Robertson, S. J. Gaffney, P. Smyth, and M. Ghil, 2007b: Cluster analysis of typhoon tracks. Part II: Large-scale circulation and ENSO. *J. Climate*, **20**(14), 3654–3676, https://doi.org/10.1175/JCLI4203.1.

Caron, L. P., M. Boudreault, and C. L. Bruyère, 2015: Changes in large-scale controls of Atlantic tropical cyclone activity with the phases of the Atlantic multidecadal oscillation. *Climate Dyn.*, **44**(7–8), 1801–1821, https://doi.org/10.1007/s00382-014-2186-5.

Chan, J. C. L., 1985: Tropical cyclone activity in the northwest Pacific in relation to the El Niño/Southern Oscillation phenomenon. *Mon. Wea. Rev.*, **113**(4), 599–606, https://doi.org/10.1175/1520-0493(1985)113<0599:TCAITN>2.0.CO;2.

Chand, S. S., and K. J. E. Walsh, 2010: The influence of the Madden-Julian Oscillation on tropical cyclone activity in the Fiji region. *J. Climate*, **23**(4), 868–886, https://doi.org/10.1175/2009JCLI3316.1.

Chen, T. C., S. P. Weng, N. Yamazaki, and S. Kiehne, 1998: Interannual variation in the tropical cyclone formation over the western North Pacific. *Mon. Wea. Rev.*, **126**(4), 1080–1090, https://doi.org/10.1175/1520-0493(1998)126<1080:IVITTC>2.0.CO;2.

Chen, T. C., S. Y. Wang, and M. C. Yen, 2006: Interannual variation of the tropical cyclone activity over the western North Pacific. *J. Climate*, **19**(21), 5709–5720, https://doi.org/10.1175/JCLI3934.1.

Delworth, T. L., and M. E. Mann, 2000: Observed and simulated multidecadal variability in the Northern Hemisphere. *Climate Dyn.*, **16**(9), 661–676, https://doi.org/10.1007/s003820000075.

ECLAC, 2009: Belize: Macro socio-economic assessment of the damage and losses caused by tropical depression 16. United Nations Economic Commission for Latin America and the Caribbean Tech. Rep.

Emanuel, K., 2005: Increasing destructiveness of tropical cyclones over the past 30 years. *Nature*, **436**(7051), 686–688, https://doi.org/10.1038/nature03906.

Frank, W. M., and G. S. Young, 2007: The interannual variability of tropical cyclones. *Mon. Wea. Rev.*, **135**(10), 3587–3598, https://doi.org/10.1175/MWR3435.1.

Girishkumar, M. S., V. P. T. Prakash, and M. Ravichandran, 2015: Influence of Pacific Decadal Oscillation on the relationship between ENSO and tropical cyclone activity in the Bay of Bengal during October–December. *Climate Dyn.*, **44**(11–12), 3469–3479, https://doi.org/10.1007/s00382-014-2282-6.

He, H. Z., J. Yang, D. Y. Gong, R. Mao, Y. Q. Wang, and M. N. Gao, 2015: Decadal changes in tropical cyclone activity over the western North Pacific in the late 1990s. *Climate Dyn.*, **45**(11–12), 3317–3329, https://doi.org/10.1007/s00382-015-2541-1.

Huang, B. Y., and Coauthors, 2017: Extended reconstructed sea surface temperature, version 5 (ERSSTv5): Upgrades, validations, and intercomparisons. *J. Climate*, **30**(20), 8179–8205, https://doi.org/10.1175/JCLI-D-16-0836.1.

Huang, P., C. Chou, and R. H. Huang, 2011: Seasonal modulation of tropical intraseasonal oscillations on tropical cyclone geneses in the western North Pacific. *J. Climate*, **24**(24), 6339–6352, https://doi.org/10.1175/2011JCLI4200.1.

Klotzbach, P. J., 2011: The influence of El Niño-Southern oscillation and the Atlantic multidecadal oscillation on Caribbean tropical cyclone activity. *J. Climate*, **24**(3), 721–731, https://doi.org/10.1175/2010JCLI3705.1.

Klotzbach, P. J., 2014: The Madden–Julian oscillation's impacts on worldwide tropical cyclone activity. *J. Climate*, **27**(6), 2317–2330, https://doi.org/10.1175/JCLI-D-13-00483.1.

Klotzbach, P. J., and E. C. J. Oliver, 2015: Modulation of Atlantic basin tropical cyclone activity by the Madden–Julian oscillation (MJO) from 1905 to 2011. *J. Climate*, **28**(1), 204–217, https://doi.org/10.1175/JCLI-D-14-00509.1.

Klotzbach, P. J., and W. M. Gray, 2008: Multidecadal variability in north Atlantic tropical cyclone activity. *J. Climate*, **21**(15), 3929–3935, https://doi.org/10.1175/2008JCLI2162.1.

Knapp, K. R., H. J. Diamond, J. P. Kossin, M. C. Kruk, and C. J. Schreck, 2018: International best track archive for climate stewardship (IBTrACS) project, Version 4. NOAA National Centers for Environmental Information, https://doi.org/10.25921/82ty-9e16.

Knapp, K. R., M. C. Kruk, D. H. Levinson, H. J. Diamond, and C. J. Neumann, 2010: The international best track archive for climate stewardship (IBTrACS): Unifying tropical cyclone data. *Bull. Amer. Meteor. Soc.*, **91**(3), 363–376, https://doi.org/10.1175/2009BAMS2755.1.

Li, R. C. Y., and W. Zhou, 2012: Changes in western Pacific tropical cyclones associated with the El Nino-Southern Oscillation cycle. *J. Climate*, **25**, 5864–5878, https://doi.org/10.1175/JCLI-D-11-00430.1.

Liu, K. S., and J. C. L. Chan, 2008: Interdecadal variability of western North Pacific tropical cyclone tracks. *J. Climate*, **21**(17), 4464–4476, https://doi.org/10.1175/2008JCLI2207.1.

Lorenz, E. N., 1956: Empirical orthogonal functions and statistical weather prediction, Scientific Report 1, Statistical Forecasting Project. Massachusetts Institute of Technology Defense Doc. Center No. 110268, 49 pp.

Lu, G. Y., and D. W. Wong, 2008: An adaptive inverse-distance weighting spatial interpolation technique. *Computers & Geosciences*, **34**(9), 1044–1055, https://doi.org/10.1016/j.cageo.2007.07.010.

Mantua, N. J., S. R. Hare, Y. Zhang, J. M. Wallace, and R. C. Francis, 1997: A Pacific interdecadal climate oscillation with impacts on salmon production. *Bull. Amer. Meteor. Soc.*, **78**(6), 1069–1080, https://doi.org/10.1175/1520-0477(1997)078<1069:APICOW>2.0.CO;2.

Murakami, H., T. L. Delworth, W. F. Cooke, M. Zhao, B. Q, Xiang, and P. C. Hsu, 2020: Detected climatic change in global distribution of tropical cyclones. *Proceedings of the National Academy of Sciences of the United States of America*, **117**(20), 10706–10714, https://doi.org/10.1073/pnas.1922500117.

Newman, M., and Coauthors, 2016: The pacific decadal oscillation, revisited. *J. Climate*, **29**(12), 4399–4427, https://doi.org/10.1175/JCLI-D-15-0508.1.

North, G. R., T. L. Bell, R. F. Cahalan, and F. J. Moeng, 1982: Sampling errors in the estimation of empirical orthogonal functions. *Mon. Wea. Rev.*, **110**(7), 699–706, https://doi.org/10.1175/1520-0493(1982)110<0699:SEITEO>2.0.CO;2.

Patricola, C. M., R. Saravanan, and P. Chang, 2014: The impact of the El Niño–Southern Oscillation and Atlantic meridional mode on seasonal Atlantic tropical cyclone activity. *J. Climate*, **27**(14), 5311–5328, https://doi.org/10.1175/JCLI-D-13-00687.1.

Peduzzi, P., B. Chatenoux, H. Dao, A. De Bono, C. Herold, J. Kossin, F. Mouton, and O. Nordbeck, 2012: Global trends in tropical cyclone risk. *Nature Climate Change*, **2**(4), 289–294, https://doi.org/10.1038/NCLIMATE1410.

Singh, O. P., 2008: Indian Ocean dipole mode and tropical cyclone frequency. *Current Science*, **94**(10), 29–31.

Sugi, M., H. Murakami, and J. Yoshimura, 2012: On the mechanism of tropical cyclone frequency changes due to global warming. *J. Meteor. Soc. Japan*, **90A**, 397–408, https://doi.org/10.2151/jmsj.2012-A24.

Van Oldenborgh, G. J., F. J. Doblas-Reyes, B. Wouters, and W. Hazeleger, 2012: Decadal prediction skill in a multi-model ensemble. *Climate Dyn.*, **38**(7), 1263–1280, https://doi.org/10.1007/s00382-012-1313-4.

Vecchi, G. A., and Coauthors, 2014: On the seasonal forecasting of regional tropical cyclone activity. *J. Climate*, **27**(21), 7994–8016, https://doi.org/10.1175/JCLI-D-14-00158.1.

Wang, B., and J. C. L. Chan, 2002: How strong ENSO events affect tropical storm activity over the Western North Pacific. *J. Climate*, **15**(13), 1643–1658, https://doi.org/10.1175/1520-0442(2002)015<1643:HSEEAT>2.0.CO;2.

Wang, B., Y. X. Yang, Q. H. Ding, H. Murakami, and F. Huang, 2010: Climate control of the global tropical storm days (1965–2008). *Geophys. Res. Lett.*, **37**(7), L07704, https://doi.org/10.1029/2010GL042487.

Wang, B., J. Liu, H.-J. Kim, P. J. Webster, S.-Y. Yim, and B. Q. Xiang, 2013: Northern Hemisphere summer monsoon intensified by mega-El Niño/southern oscillation and Atlantic multidecadal oscillation. *Proceedings of the National Academy of Sciences of the United States of America*, **110**(14), 5347–5352, https://doi.org/10.1073/pnas.1219405110.

Wang, B., and Coauthors, 2018: Toward predicting changes in the land monsoon rainfall a decade in advance. *J. Climate*, **31**(7), 2699–2714, https://doi.org/10.1175/JCLI-D-17-0521.1.

Wang, C., L. G. Wu, H. K. Zhao, J. Cao, and W. Tian, 2019: Is there a quiescent typhoon season over the western North Pacific following a strong El Niño event? *International Journal of Climatology*, **39**(1), 61–73, https://doi.org/10.1002/joc.5782.

Webster, P. J., G. J. Holland, J. A. Curry, and H.-R. Chang, 2005: Changes in tropical cyclone number, duration, and intensity in a warming environment. *Science*, **309**(5742), 1844–1846, https://doi.org/10.1126/science.1116448.

Wu, L. G., B. Wang, and S. Q. Geng, 2005: Growing typhoon influence on East Asia. *Geophys. Res. Lett.*, **32**(18), L18703, https://doi.org/10.1029/2005GL022937.

Xiang, B., and B. Wang, 2013: Mechanisms for the advanced Asian Summer Monsoon onset since the mid-to-late 1990s. *Journal of Climate*, **26**, 1993–2009, https://doi.org/10.1175/JCLI-D-12-00445.1.

Xiao, D. and J. P. Li, 2007: Spatial and temporal characteristics of the decadal abrupt changes of global atmosphere-ocean system in the 1970s. *J. Geophys. Res.*, **112**(D24), D24S22, https://doi.org/10.1029/2007JD008956.

Yu, J. H., Y. Q. Wang, and K. Hamilton, 2010: Response of tropical cyclone potential intensity to a global warming scenario in the IPCC AR4 CGCMs. *J. Climate*, **23**(6), 1354–1373, https://doi.org/10.1175/2009JCLI2843.1.

Zhan, R. F., Y. Q. Wang, and X. T. Lei, 2011: Contributions of ENSO and East Indian Ocean SSTA to the interannual variability of Northwest Pacific tropical cyclone frequency. *J. Climate*, **24**(2), 509–521, https://doi.org/10.1175/2010JCLI3808.1.

Zhang, Q., L. G. Wu, and Q. F. Liu, 2019: Tropical cyclone damages in China 1983-2006. *Bull. Amer. Meteor. Soc.*, **90**(4), 489–496, https://doi.org/10.1175/2008BAMS2631.1.

Zhang, Y., J. M. Wallace, and D. S. Battisti, 1997: ENSO-like interdecadal variability: 1900–93. *J. Climate*, **10**(5), 1004–1020, https://doi.org/10.1175/1520-0442(1997)010<1004:ELIV>2.0.CO;2.

Zhang, Y., S. P. Xie, Y. Kosaka, and J. C. Yang, 2018: Pacific decadal oscillation: Tropical pacific forcing versus internal variability. *J. Climate*, **31**(20), 8265–8279, https://doi.org/10.1175/JCLI-D-18-0164.1.

Zhao, H. K., and C. Z. Wang, 2016: Interdecadal Modulation on the Relationship between ENSO and Typhoon Activity during the Late Season in the Western North Pacific. *Climate Dyn.*, **47**(12), 315–328, https://doi.org/10.1007/s00382-015-2837-1.

Zhao, H. K., and C. Z. Wang, 2019: On the relationship between ENSO and tropical cyclones in the western North Pacific during the boreal summer. *Climate Dyn.*, **52**(1-2), 275–288, https://doi.org/10.1007/s00382-018-4136-0.

Zhao, H. K., L. G. Wu, and W. C. Zhou, 2010: Assessing the influence of the ENSO on tropical cyclone prevailing tracks in the western North Pacific. *Adv. Atmos. Sci.*, **27**(6), 1361–1371, https://doi.org/10.1007/s00376-010-9161-9.